Express Polymer Letters Vol.16, No.12 (2022) 1253–1266
Available online at www.expresspolymlett.com
https://doi.org/10.3144/expresspolymlett.2022.91

Research article

Phase transition and crystallization behavior of grafted starch nanocrystals in PLA nanocomposites

Somayeh Sharafi Zamir[1,2*], *Babak Fathi*[1], *Abdellah Ajji*[3], *Mathieu Robert*[1], *Said Elkoun*[1]

[1]Center for Innovation in Technological Eco-design (CITÉ), University of Sherbrooke, J1K 2R1 Sherbrooke, Qc, Canada
[2]Chemistry Department, McGill University, Sherbrooke West, H3A 0B9 Montreal, Qc, Canada
[3]Chemical Engineering Department, Polytechnique de Montreal, H3C 3A7 Montreal, Qc, Canada

Received 4 April 2022; accepted in revised form 20 July 2022

Abstract. Polylactic acid (PLA) has shown two different crystalline structures, namely α and α′ when cooled down from the melt state. However, α-PLA has shown significant improvement in the barrier and mechanical properties of PLA. Although the effect of some nucleating agents on phase transformation of the PLA has been determined in the past, this is the first attempt, the effect of the starch nanocrystals on the formation of polymorphic crystal structure of PLA was evaluated. In this framework, the effect of lactic acid grafted starch nanocrystals (SNCs-*g*-LA) concentrations on the phase transition, and crystallization behavior of PLA/SNCs-*g*-LA nanocomposites at different isothermal crystallization temperatures (T_c) were studied. The results indicate that SNCs-*g*-LA nanoparticles promote the degree of crystalline transition to yield the highly crystalline ordered α-PLA. Further, the half-time crystallization ($t_{1/2}$) of PLA composites was calculated by the Avrami equation. The $t_{1/2}$ of PLA was minimum by adding 5 wt% SNCs-*g*-LA nanoparticles, and it decreased from 10.4 to 3.9 min. The growth rate of the spherulite morphology of PLA composites showed a significant improvement in the crystalline structure of PLA/SNCs-*g*-LA (5 wt%) nanocomposites as well.
Finally, small angle X-ray scatting (SAXS) analysis showed that the inclusion of 5 wt% grafted SNCs resulted in the increment of the long period (L_{ac}) as well as crystal layer thickness (L_c).

Keywords: *biodegradable polymers, phase transition, crystallinity, thermal properties, nanomaterials*

1. Introduction

The development of bio-based and biodegradable polymers is an important step towards the replacement of traditional synthetic plastic materials with natural resources [1]. Among the different bio-based polymers, poly(lactic acid) (PLA) has been a subject of many previous investigations due to its commercial availability and various applications in different domains such as medical, food packaging film, and automotive industry [1–5]. It has been shown that PLA, polyhydroxyalkanoate (PHA), polybutylene succinate (PBS), polybutylene adipate therephthalate (PBAT), and others constitute over 55.5% of bioplastic production globally [6]. PLA has high strength and good optical and physical properties compared to the most common type of petroleum-based polymers, such as polystyrene (PS) and polyethylene terephthalate (PET) [7, 8]. PLA exhibits two different crystalline structures, namely α and α′ structures when cooled from the melt state. The α structure of PLA is a highly ordered crystalline structure compared to the α′ structure (slightly altered crystal structure) [9, 10]. This change in the conformational structure of α′ and α structure can affect several physical properties such as gas permeability and mechanical properties [11, 12]. It was postulated the α structure in PLA has lower water vapor and oxygen permeability than α′ structure due to the more packed crystalline

*Corresponding author, e-mail: somayeh.sharafizamir@mail.mcgill.ca

structure, which is very important for food packaging applications [11]. This compact arrangement also affects the mechanical properties such as Young's modulus and the elongation at break [12]. However, PLA has some shortcomings that do not fulfill all the prerequisites of the food packaging industry. It has been demonstrated that the slow crystallization rate and low level of crystallinity of PLA decreased the melting strength, which led to a failure in polymer processing [11, 12]. Hence, many researchers are working toward finding more efficient ways to enhance the PLA crystallization kinetics and increase its degree of crystallinity. Two well-documented approaches to increase the crystallinity of PLA have been reported; a) by manipulating the intrinsic characteristics of PLA, such as the ratio between two enantiomers (L- to D-lactide) [13] and molecular weight [14] and b) by adding nucleating agents [15], plasticizer [16] and/or both nucleating agents and plasticizer together [17].

Adding nucleating agents is an effective way to create more surface area and decrease the surface free energy barrier for nucleation. Therefore, they are applied to accelerate the nucleation rate and the growth of spherulites, which will result in a short processing time [18–25]. In addition, the amount, size, and surface crystalline morphology of nucleating agents can determine not only the rate of crystallinity but also the type, size, and morphology of spherulites of semicrystalline polymers [18–25]. The nucleating agents are also used to control the crystalline conformation of polymorphic polymers such as PLA [18–25]. Besides, adding nucleating agents can improve other properties such as thermal resistance, impact strength, optical transparency, and barrier properties [18–25]. However, only a few nucleating agents have been developed for PLA to control crystalline conformation and to enhance the kinetics of crystallization of PLA at the same time, including; graphene nanosheet (GNSs) [26], dibenzylidene-D-sorbitol (DBS) [27] and uracil [28]. Xu *et al.* [26] demonstrated that the presence of graphene nanosheet (GNSs) resulted in more α′ structure in PLLA nanocomposite than α structure [26]. They also showed that the phase transition temperature of PLLA/GNSs shifted to a higher temperature compared to neat PLLA [26]. Lai *et al.* [27] investigated the effect of 1–4 wt% of dibenzylidene-D-sorbitol (DBS) on the thermal and crystalline behavior of PLLA. They found that the ordered and stable form (α structure) is favored in PLLA/DBS nanocomposites, and phase transition temperature shifted to a lower temperature as more DBS content was added. Pan *et al.* [28] reported that the addition of uracil enhances the crystallization rate, and it also controls the crystalline morphology of PHB copolymers. Nevertheless, most of these chemicals are not biocompatible, biodegradable, and non-toxic; therefore, their composition of them with PLA is not desirable in the utilization of the final product.

Among different bio-based fillers, starch has attracted widespread attention due to its availability, renewability, and being cheaper than most of the nucleating agents tested [29]. It has been demonstrated that the incorporation of starch in the PLA matrix has several other secondary benefits, such as higher mechanical strength, better mechanical behavior, and lower gas permeability [29–31]. Jacobsen *et al*. [16] studied the effect of dry starch on the non-isothermal crystallization behavior of PLA. They reported that the dry starch did not influence the crystallization of PLA [16]. Nevertheless, Ke and Sun [32] showed that dry starch could significantly increase the crystallinity of PLLA, having 8% D-concentrations. They demonstrated that the addition of dry starch to PLLA reduces $t_{1/2}$ from 13.6 to 3.2 min [32].

Starch nanocrystals (SNCs) are the crystalline phase of starch granules that are mainly produced by acid hydrolysis of the amorphous phase of starch grains [33, 34]. SNCs have attracted many interests because they are unique in their morphology, good mechanical properties, and high reactivity [33, 34]. It has been proposed that the introduction of modified SNCs into the PLA matrix can affect the permeability and mechanical properties of PLA more than starch powder [35]. For example, the addition of starch nanocrystal-*graft*-poly(ε-caprolactone) (PCL-*g*-SNCs) into PLA resulted in enhancement of elongation at break and, at the same time lowering the Young's modulus [36]. However, only a few studies have investigated the potential of SNCs as a nucleating agent for PLA [37]. To the best of our knowledge, there have been a few studies done on the effect of SNCs on the crystallization of PLA, however, the role of SNCs-*g*-LA on the crystalline structures, transcrystallization, and crystallization behavior of PLA was not studied.

This work aims to determine the effect of SNCs-*g*-LA on the kinetics of crystallization and the formation of polymorphic crystals of PLA. In this regard, LA molecules are grafted onto the surfaces of SNCs

through a simple esterification reaction. Then the effect of SNCs-*g*-LA concentrations [wt%] on the crystallization behavior, including nucleation and spherulitic growth rate of PLA, melting behavior, and crystalline conformation of PLA were investigated., The effect of SNCs-*g*-LA nanoparticles content on the crystalline structure and melting behavior of PLA composites were investigated by wide angle X-ray diffraction (WAXS) and differential scanning calorimetry (DSC). Subsequently, the effect of different concentrations of SNCs-*g*-LA on the nucleation and overall crystallization rate of PLA composites were measured using DSC. Finally, the effect of SNCs-*g*-LA nanocomposites on the morphology and spherulite growth rate are examined by polarized optical microscopy (POM).

2. Experimental sections

2.1. Materials

Semi-crystalline commercial-grade PLA (4032D) pellets were supplied by Nature Works LLC (Minnesota, USA), and it has 2% of D-lactide content. The average molecular weight (M_w) and polydispersity index (M_w/M_n) of PLA pellets were about 109 kg/mol and 1.57, respectively. In addition, corn starch and LA were purchased from Sigma-Aldrich, Canada, and it was majorly contained amylopectin.

2.2. Extraction of starch nanocrystals (SNCs)

Starch nanocrystals (SNCs) were prepared by acid hydrolysis of corn starch according to the previously reported work of authors [34, 46]. Briefly, 147 g corn starch granules were dispersed into a 500 ml of 3.16 M aqueous sulfuric acid (H_2SO_4). The suspension was then kept under mechanical stirring at a speed of 400 rpm and a temperature of 40 °C for 5 days. Subsequently, the resulting solution was washed in distilled water at 11 °C by successive centrifugation (Centrifuge 6K-15C, Sigma) at 10 000 rpm until a neutral pH was obtained. The suspension was then freeze-dried using a Heto Power Dry PL6000 apparatus from Thermo Fisher Scientific. After freeze-drying, a few drops of chloroform were added to the SNCs powder to avoid bacterial activity, and then SNCs were kept in the cold environment at 4 °C.

2.3. Chemical modification of SNCs

Surface modification of SNCs by LA was carried out as the following: in brief, 30 g of starch nanoparticles were first dispersed into the 100 ml of tetrahydrofuran (THF). Then, LA was added slowly to the reaction mixture. The resulting reaction mixture was heated up to 60 °C and maintained at this temperature for 30 mins under an argon atmosphere. After THF evaporation, 150 ml toluene was slowly added to the mixture, and it was heated up to 85 °C and kept at this temperature for 24 hrs. Finally, the reaction mixture was centrifuged at 10 000 rpm for 20 min, to remove the toluene, and it was washed with THF and ethyl acetate to remove the toluene remaining in the reaction product. The final product was then dried under a vacuum at 45 °C.

2.4. Preparation of PLA/SNCs-*g*-LA nanocomposites

The PLA/SNCs-*g*-LA nanocomposites were prepared by the solvent casting process and evaporation technique. Initially, PLA was dissolved in dichloromethane solvent at 70 °C, and then different concentrations of SNCs-*g*-LA (3, 5, and 7 wt%.) were added to the PLA solution, and the solution was stirred for 24 h. Subsequently, the solution of PLA/ SNCs-*g*-LA was dried by the casting process. Finally, the prepared nanocomposite films were vacuum dried overnight to remove the traces of the solvents.

2.5. Methods

2.5.1. Fourier-transform infrared spectroscopy (FT-IR)

Fourier transform infrared spectroscopy (FT-IR) analysis was performed to determine the different functional groups present on the surface of SNCs before and after grafting with LA. The FT-IR analysis was performed using a JASCO-4600 spectrometer (Japan) in the range of 4000–600 cm^{-1} with a resolution of 4 cm^{-1}.

2.5.2. Differential scanning calorimetry (DSC)

The thermal behavior of neat PLA and PLA/SNCs-*g*-LA nanocomposites was studied by a Q2000, TA instrument, differential scanning calorimeter (DSC) Q2000, TA Instruments, equipped with a liquid nitrogen cooling system. Prior to the measurements, the temperature was calibrated using indium as the standard material. Samples (5–10 mg) were sealed in a closed aluminum pan. Afterward, the samples were heated from room temperature up to 200 °C with a heating rate of 10 °C/min for 3 min to eliminate any possible crystallinity or residual stress in the samples. Then samples were directly quenched to different

crystallization temperatures (T_c = 80–130 °C) to allow them to crystallize from melt under quiescent conditions. The temperature was then ramped back up to 200 °C with a heating rate of 10 °C/min to probe the melting behavior after the crystallization process.

2.5.3. Wide angle X-ray diffraction (WAXD)

The crystalline structures of neat PLA and PLA/SNCs-*g*-LA nanocomposites were analyzed at the T_c by the wide-angle X-ray Diffraction (WAXD), D-8, Bruker. The samples were exposed to an X-ray beam with the X-ray generators running at 40 kV and 40 mA. The copper K_α radiation (k = 1.542 Å) was selected, and the scanning was carried out at 0.03°/s in the angular region (2θ) of 5–40°.

2.5.4. Polarized optical microscopy (POM)

The spherulite growth rate of neat PLA and PLA nanocomposites was observed using polarized optical microscopy (POM), Nicon 249171, in conjunction with the hot-stage (Mettler Toledo FP82HT). Samples were prepared by cutting small pieces from prepared films. Then, the sample was placed between two microscopy slides and pressed gently to form a thin film (~20–50 μm). Initially, the hot stage was stabilized at 200 °C, and then samples were kept at 200 °C for 3 min before any thermal protocol. After that, the sample was quenched to different isothermal temperate (T_c = 80–130 °C) and continued at that temperature for one hour. The hot stage is calibrated with a melting point standard of ±0.2 °C accuracy.

2.5.5. Small angle X-ray scattering (SAXS)

Small angle X-ray scattering (SAXS) patterns were collected with a Bruker SAXS Nanostar system, equipped with a microfocus copper anode at 45 kV/0.65 mA, MONTAL OPTICS, and VANTEC 2000 2D detector. The distance from the detector to the sample was calibrated with a silver behenate standard prior to the measurements. The scattering intensities were integrated from 0.1 to 2.8°. Collection exposure times were 500 seconds.

3. Results and discussions

3.1. FT-IR analysis

The FT-IR spectra of neat SNCs and SNCs-*g*-LA nanoparticles are shown in Figure 1. The FT-IR spectrum of neat SNCs show characteristic peaks of stretching and bending vibrations of –OH groups at the wavelengths of 1650 and 3300 cm^{-1} [47]. Moreover,

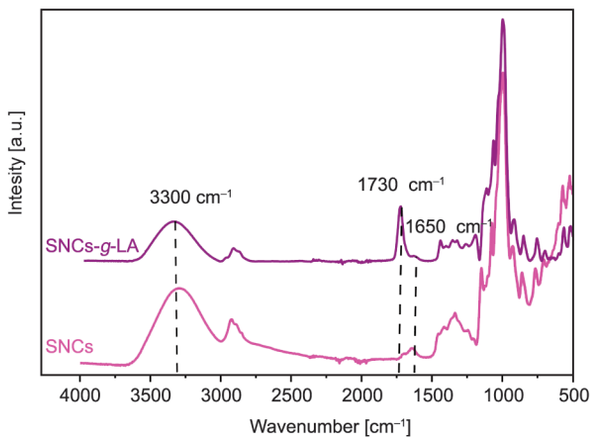

Figure 1. FT-IR spectra of SNCs and SNCs-*g*-LA nanoparticles.

the stretching vibration of C–O bonding in C–O–H and C–O–C groups of the glycosidic rings appear at the wavelength of 1150, 1080, and 990 cm^{-1}, respectively [47]. After grafting SNCs by LA, an additional sharp peak appeared at 1730 cm^{-1}. This peak is attributed to the carbonyl stretching group (=CO), which is present in the lactic acid. In addition, two new peaks at 1250 and 1055 cm^{-1} were observed that can be attributed to C–O group presenting an ester group. Moreover, grafted SNCs demonstrate a decrease in the peak intensity of –OH functions around the wavelengths of 1650 and 3300 cm^{-1}. All these results imply a successful bonding of the LA molecules on the SNCs surface.

3.2. Wide angle X-ray scattering (WAXS)

To determine the phase transition temperature (T_{trans}) and crystalline structures of neat PLA and PLA/SNCs-*g*-LA nanocomposites, WAXS analysis was performed after crystallization of samples at different T_c. Figure 2 shows the WAXS patterns of isothermally crystallized neat PLA and PLA with 3, 5, and 7 wt% of SNCs-*g*-LA nanoparticles after crystallization at the different T_c (80–130 °C). As can be seen in Figure 2d, distinct diffraction peaks were observed for isothermally crystallized neat PLA samples at the different T_c, preferably from 80 to 130 °C. At T_c above 120 °C, five diffraction peaks are observed at 2θ = 11.1, 14.5, 16.5, 19.5 and 22.5°. These diffraction peaks can be attributed to the (103)/(004), (010), (110)/(200), (203)/(113) and (210) planes of PLA α structure respectively [9, 10, 38]. However, the intensity of diffraction peaks at the 2θ = 11.1, 14.5, and 22.5° decreases with decreasing T_c to 100 °C, and finally, these diffraction peaks disappear at $T_c \leq$ 100 °C.

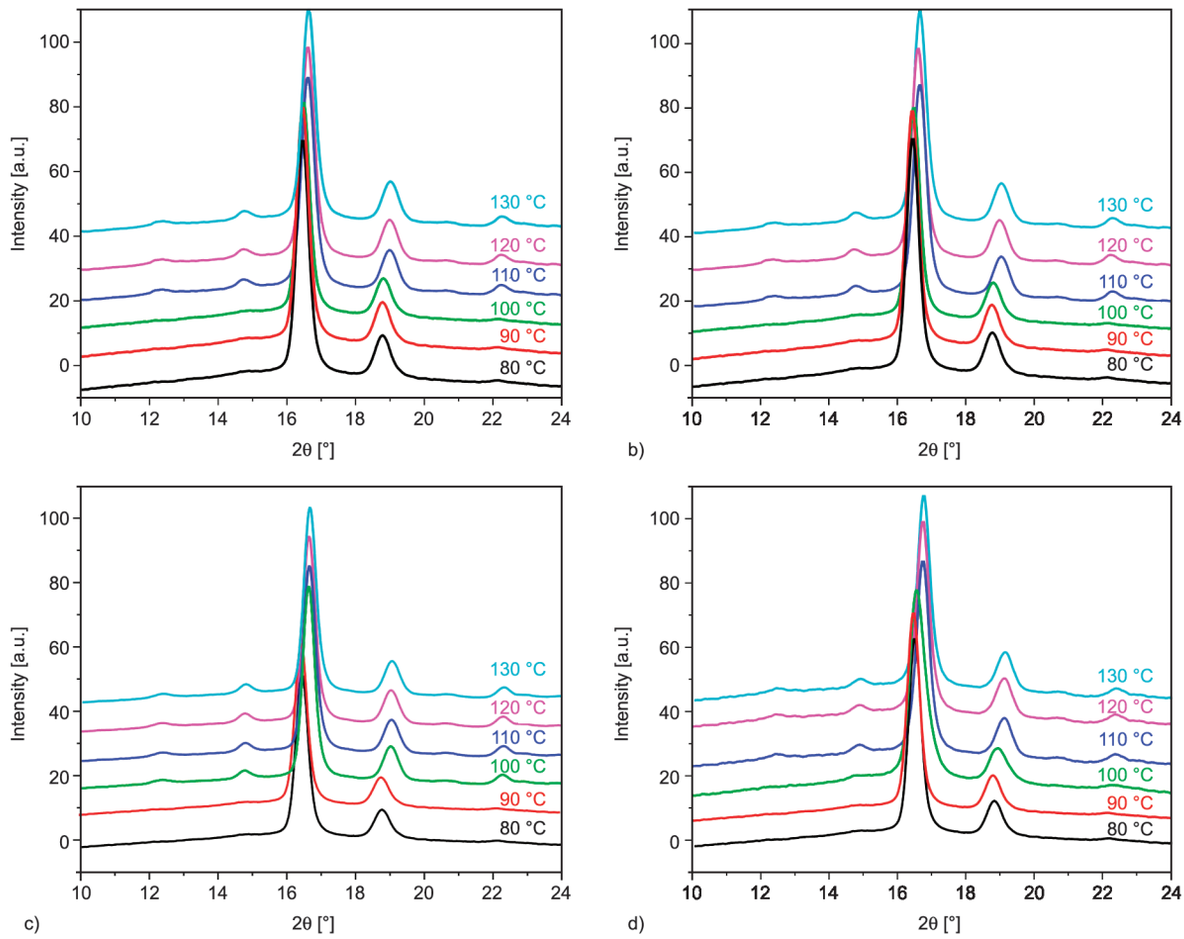

Figure 2. WAXS patterns of a) neat PLA, b) PLA/SNCs-*g*-LA (3 wt%), c) PLA/SNCs-*g*-LA (5 wt%) and d) PLA/SNCs-*g*-LA (7 wt%) nanocomposites at different isothermal crystallization temperatures.

At the same time, the 2θ value of 16.5 and 19.5° of diffraction peaks shifted to the lower value evidenced in the WAXS patterns. The appearance of the diffraction peaks at 2θ = 11.1, 14.5, and 22.5° and the subsequent shifting of the two diffraction peaks at 2θ = 16.5 and 19.5° to lower 2θ at the same temperature is related to the presence of both α and α′ structures of PLA [9, 10, 38]. Finally, at T_c = 80 °C the 2θ of 16.5 and 19.5° diffraction peaks shifted to the lower values, which is attributed to the presence of PLA α′ structure [9, 10, 38].

The comparison of WAXS profiles of PLA/SNCs-*g*-LA nanocomposites with neat PLA confirms that the characteristics of α and α′ structures are observed in WAXS pattern of all PLA/SNCs-*g*-LA nanocomposites. However, the 2θ value of diffraction peaks for (110)/(200) and (203)/(113) planes shifts to a higher value with adding SNCs-*g*-LA nanoparticles. These changes in the 2θ angle indicate a higher phase transition from α′ to α structure till only α structure is present. More importantly, it was found that the T_{trans} of α′ to α structure is minimum when 5 wt% SNCs-*g*-LA nanoparticles were added into PLA. However, a further decrease in SNCs-*g*-LA nanoparticles loading (*i.e.*, 3 wt%) resulted in an increase in the T_{trans} temperature. It seems that 5 wt% of SNCs-*g*-LA loading has a considerable effect on the T_{trans}, which got reduced to 100 °C compared to 110 °C as reported in the case of neat PLA. This means that SNCs-*g*-LA was helpful in forming the more stable crystal structure (α) instead of the less stable crystal structure (α′) in PLA matrix and promoted superior crystalline structure in PLA at lower T_c by adding 5 wt% SNCs-*g*-LA nanoparticles.

Figure 3 shows the variation of lattice spacing of the (110)/(200) diffractions ($d_{110/200}$) calculated from the Braggs law for neat and PLA nanocomposites. The results show that the $d_{110/200}$ values of α′ crystal structure of neat PLA are higher compared to the SNCs-*g*-LA reinforced PLA nanocomposites. While by increasing T_c to 120 °C, the $d_{110/200}$ values decrease further for the neat PLA and PLA nanocomposites regardless of the grafted SNCscontent. However, the SNCs-*g*-LA has more influence on the

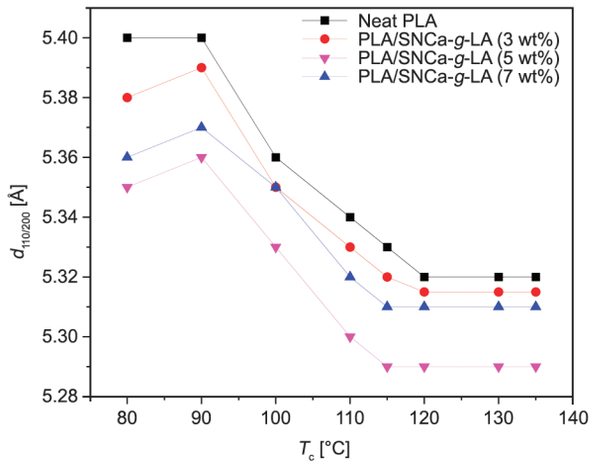

Figure 3. The lattice spacing of the (110)/(200) diffractions ($d_{110/200}$) of neat PLA and PLA nanocomposites with different concentrations.

$d_{110/200}$ values of α crystal of neat PLA, which is crystallized above T_c =120 °C where just α crystal structure is formed. This means that SNCs-*g*-LA affects not only the $d_{110/200}$ value of α′ crystal structure but also the $d_{110/200}$ of α crystal structure of PLA. The enhancement of $d_{110/200}$ of α crystal structure is most predominant when 5 wt% SNCs-*g*-LA nanoparticles were added to neat PLA.

3.3. Differential scanning calorimetry (DSC)

It has been shown that the melting behavior of semi-crystalline polymers such as PLA has a direct relationship with their crystal structures [39]. Therefore, the melting behavior of both PLA and PLA nanocomposites was studied using DSC analysis. Figure 4 shows the melting behavior of isothermally crystallized neat and PLA/SNCs-*g*-LA nanocomposites at a wide range of T_c (80–130 °C), and subsequently, samples were melted above the T_m of PLA (200 °C). Three different melting behaviors were observed in the DSC thermograms irrespective of the sample: i) a single endothermic melting peak above 120 °C, ii) a secondary endothermic peak that appears before the main endothermic melting peak at the temperature

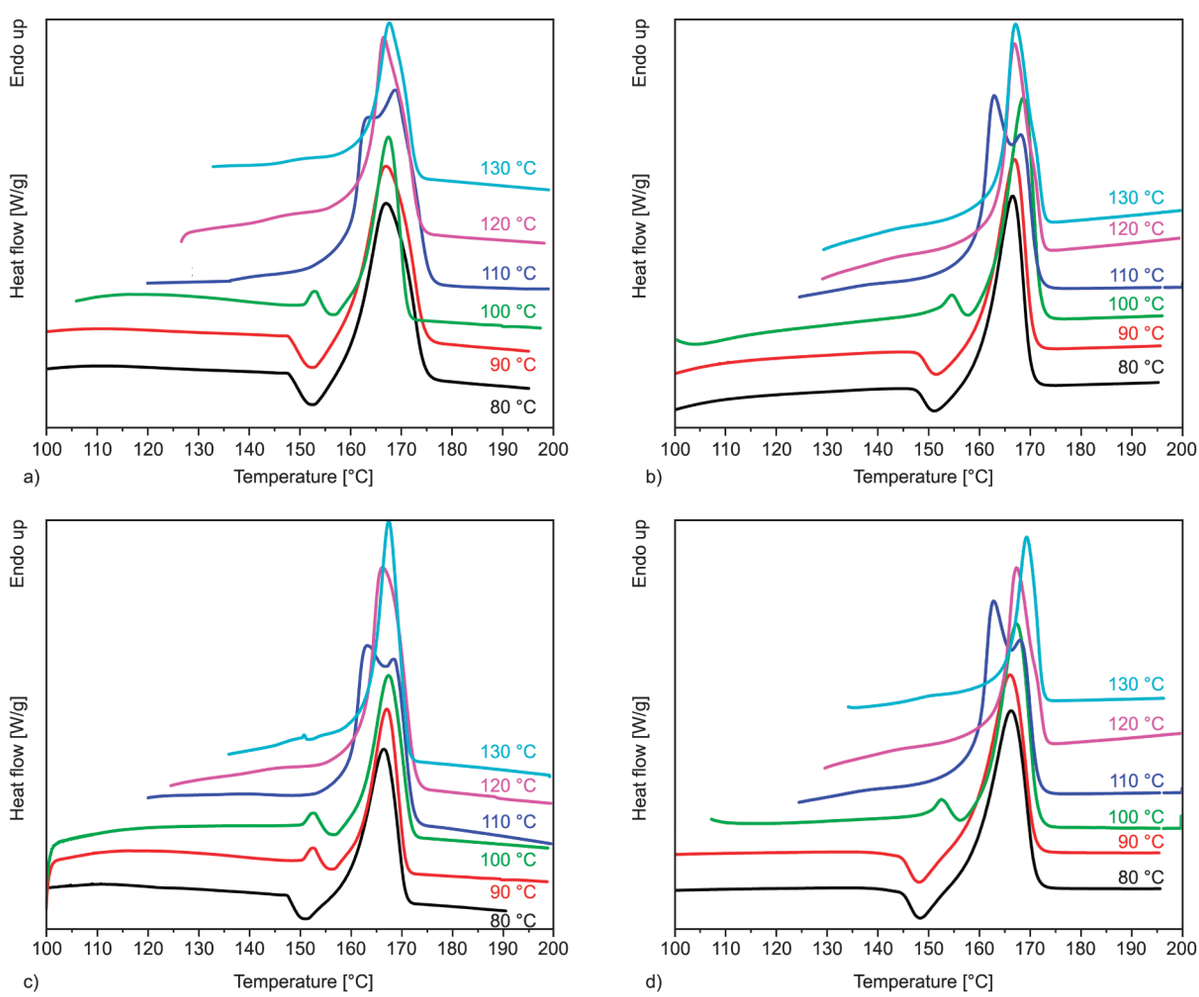

Figure 4. Melting behaviour of a) neat PLA, b) PLA/SNCs-*g*-LA (3 wt%), c) PLA/SNCs-*g*-LA (5 wt%) and d) PLA/SNCs-*g*-LA (7 wt%) nanocomposites at different isothermal crystallization temperatures.

range of 100–120 °C, iii) an additional small exothermic peak that appears just before the main endothermic peak (below 100 °C). As mentioned previously in WAXS results, neat PLA, which is crystallized between 110 °C < T_c < 120 °C shows a transition from α′ to α structure. Furthermore, for neat PLA crystallized at T_c below 110 °C and above 130 °C only α′ and α structure was observed, respectively. Since α′ structure is less ordered than α structure, thus the melting point of PLA α′ structure is lower than α structure. As can be seen in Figure 4a, the neat PLA is isothermally crystallized at 80 °C, and has a lower melting temperature (166.0 °C) than the one which is isothermally crystallized at 130 °C (168.8 °C). This means that the crystal structure of a sample which is isothermally crystallized at 80 and 130 °C are different. According to the melt recrystallization theory [32], although the higher melting temperature (168.8 °C) can be solely attributed to the melting of α structure, the lower melting temperature (166.0 °C) cannot be uniquely attributed to the α′ structure. Therefore, the exothermic peak which appears before the main endothermic peak of the PLA sample is isothermally crystallized at 80 °C and is suspected to be related to the transition of α′ to α structure [40]. For PLA samples crystallized between 100–110 °C, a small endothermic peak disappeared, and a double melting peak was observed in the DSC thermograms. However, at T_c above 120 °C, the two melting peaks collapse, and a single sharp endothermic peak is observed. In the case of PLA nanocomposites, very similar T_c-dependent DSC thermograms were observed. However, a small exothermic peak starts to disappear at T_c = 90 °C, which is 10 °C lower than neat PLA (100 °C). This indicates that the addition of SNCs-*g*-LA nanoparticles encourages the PLA molecular chains to arrange themselves in a more ordered form (α structure) at a lower temperature. Furthermore, the melting temperature of PLA nanocomposite samples isothermally crystallized at 130 °C is higher than the neat PLA sample isothermally crystallized at the same temperature. Indicating that more α structure is present in PLA nanocomposite compared to neat PLA especially when 5 wt% of SNCs-*g*-LA is added into the PLA matrix.

The equilibrium melting temperature (T_m^0) of both neat and PLA nanocomposites was calculated by the Hoffman-Weeks theory [41]. The T_m^0 was measured based on the extrapolation of the linear part of the T_m above 110 °C since at above this temperature T_m are considered to relate to the melting point of the α structure. Figure 5 shows the T_m^0 as a function of T_c of neat PLA and PLA nanocomposites containing 3, 5, and 7 wt% SNCs-*g*-LA nanoparticles. Neat PLA exhibits T_m^0 at 187.5 °C in this condition which is reported by Zhang *et al.* [10] as well. The [10] of PLA was influenced significantly by the concentration levels of SNCs-*g*-LA nanoparticles. Regardless of the different amounts of grafted SNCs present, the T_m^0 in the PLA nanocomposites is smaller than neat PLA. The addition of 3, 5, and 7 wt% of SNCs-*g*-LA nanoparticles decreases the T_m^0 to 185.4, 183.7, and 185.9 °C, respectively. This decrease indicates the formation of the perfect crystalline and ordered structure at lower under cooling. As can be seen, the addition of 5 wt% SNCs-*g*-LA nanoparticles resulted in more decrement in T_m^0, while increasing the concentration of grafted SNCs was unfavorable and induced higher T_m^0. Therefore the phase transition temperature is lowered with decreasing SNCs-*g*-LA nanoparticles concentrations to 5 wt%.

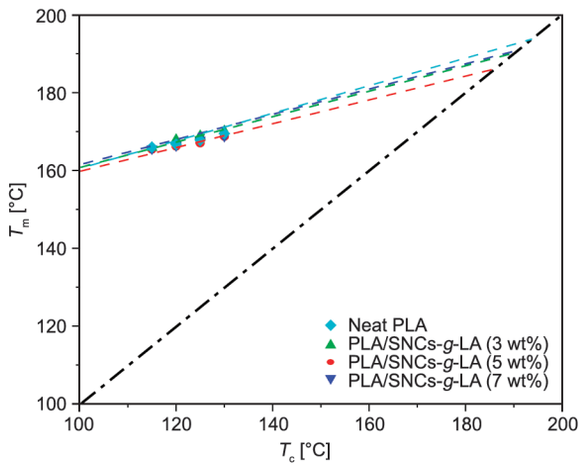

Figure 5. Equilibrium melting point of neat PLA and PLA nanocomposites with different concentrations of SNCs-*g*-LA nanoparticles ranging from 3 to 7 wt%.

3.4. Effect of SNCs-*g*-LA nanoparticles on the nucleation rate of PLA

The influence of SNCs-*g*-LA nanoparticles concentrations (3, 5, and 7 wt%) on the overall isothermal crystallization behavior and kinetics of PLA were studied by using DSC. Then, the relative degree of crystallinity ($X(t)$) was quantified theoretically by the Avrami equation at different T_c using the Equation (1) [42]:

$$X(t) = 1 - \exp(-kt^n) \quad (1)$$

where k is the crystallization rate constant, and n is the Avrami exponent, which depends on the nucleation and growth mechanisms of crystallites.
The Avrami parameters (n and k) can be calculated using the Equation (2):

$$\ln\left(-\ln\left[1-X(t)\right]\right) = n\ln(t) + \ln k \tag{2}$$

Figure 6 shows the plot of $\ln[-\ln(1-X(t)]$ *versus* $\ln(t)$ of neat and PLA nanocomposites at different T_c. In all samples, Avrami plots were found to be linear, demonstrating the accuracy of the procedure as shown in Figure 6. The slope of the line in the plot of $\ln[-\ln(1-X(t)]$ *versus* $\ln(t)$ gives the value of n. Subsequently, the crystallization rate constant (k) can be obtained using the Equation (3):

$$k = \frac{\ln 2}{t_{1/2}^{n}} \tag{3}$$

where $t_{1/2}$ is the half-time of crystallization which is defined as a time when $X(t)$ reaches half of the crystallization. Table 1 summarizes the effect of SNCs-*g*-LA concentrations on the n and k values and $t_{1/2}$. Avrami exponent (n) for polymer crystallization is usually between 2 and 4, and it is related to the type of nucleation and geometry of crystal growth [37]. As shown in Table 1, the value of n decreases and then increases with increasing T_c or with decreasing undercooling. The depletion of the n value is related to the heterogeneous mechanism of nucleating agents (*i.e.*, dimensional of nuclei) and spherulite parameters (*i.e.*, spherulite morphology). Furthermore, in both neat PLA and PLA nanocomposites, the value of k decreases with increasing T_c, revealing that the nucleation is controlled by the crystallization process because of the low undercooling degree present in the current experimental temperatures. However, the crystallization constant k of PLA nanocomposites is greater than that of the neat PLA at the equivalent temperature, which indicates that the crystallization rate of PLA nanocomposites is higher than that of the neat PLA. The value of k

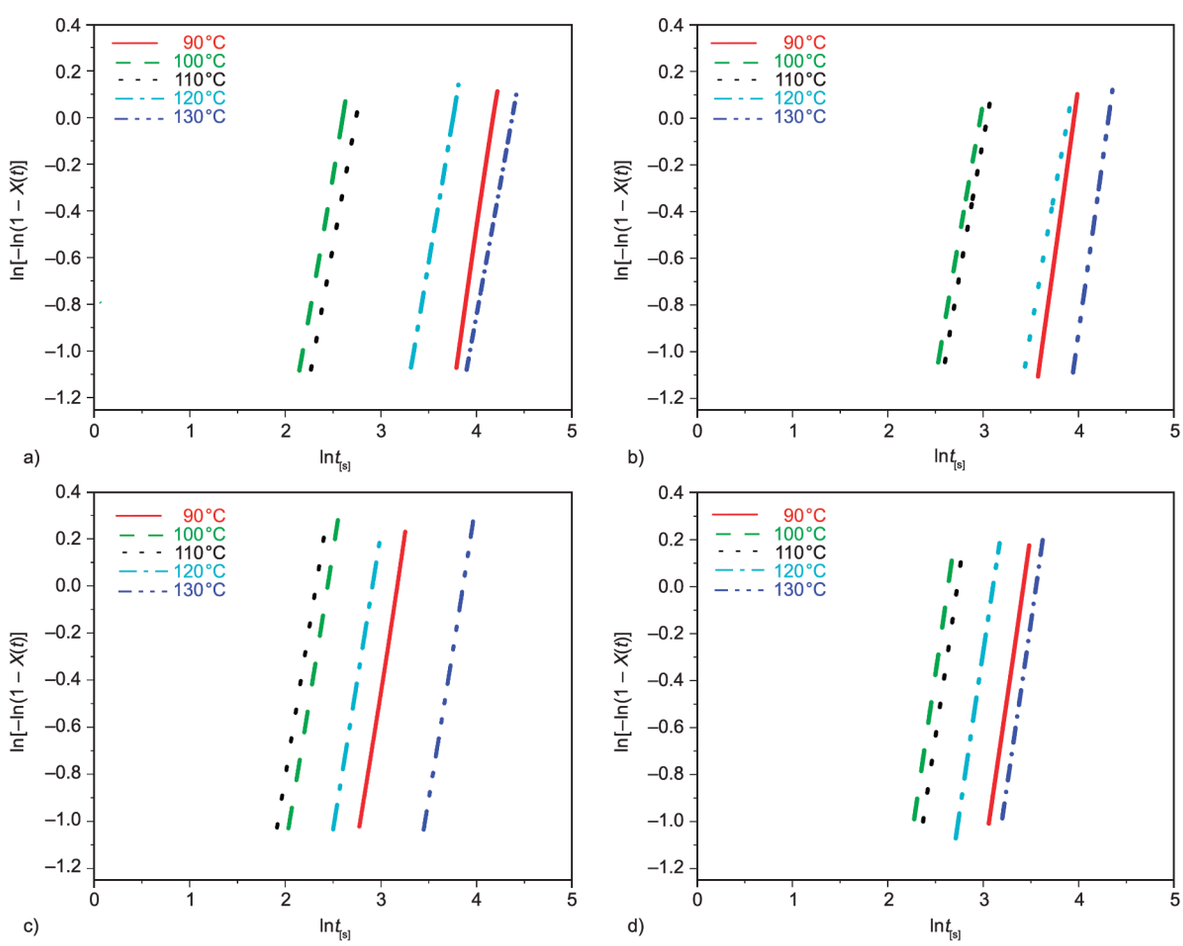

Figure 6. Plot of $\ln[-\ln(1-X(t)]$ *versus* $\ln(t)$ of neat PLA and PLA nanocomposites with different concentrations. a) neat PLA, b) PLA/SNCs-*g*-LA (3 wt%), c) PLA/SNCs-*g*-LA (5 wt%) and d) PLA/SNCs-*g*-LA (7 wt%) at different isothermal crystallization temperatures.

Table 1. The effect of SNCs-*g*-LA nanoparticles concentrations on n and k values of PLA.

Samples	PLA			PLA/SNCs-*g*-LA (3 wt%)			PLA/SNCs-*g*-LA (5 wt%)			PLA/SNCs-*g*-LA (7 wt%)		
T_c [°C]	$t_{1/2}$	*n*	*k*	$t_{1/2}$	*n*	*k*	$t_{1/2}$	*n*	*k*	$t_{1/2}$	*n*	*k*
80	43.0	3.3	$2.8208 \cdot 10^{-5}$	23.0	2.5	$2.7321 \cdot 10^{-4}$	12.0	2.5	$1.3895 \cdot 10^{-3}$	15.0	3.0	$2.0537 \cdot 10^{-4}$
90	22.0	3.3	$2.5753 \cdot 10^{-5}$	18.6	2.5	$4.6456 \cdot 10^{-4}$	10.8	2.4	$2.2940 \cdot 10^{-3}$	12.5	3.0	$3.5489 \cdot 10^{-4}$
100	13.5	2.5	$1.0351 \cdot 10^{-3}$	10.3	2.6	$1.6123 \cdot 10^{-3}$	3.9	2.4	$2.2830 \cdot 10^{-2}$	5.5	2.8	$5.8580 \cdot 10^{-3}$
110	10.4	2.5	$1.9872 \cdot 10^{-3}$	12.0	2.6	$1.0838 \cdot 10^{-4}$	5.1	2.4	$1.3880 \cdot 10^{-2}$	7.2	2.8	$2.2830 \cdot 10^{-3}$
120	16.6	2.8	$2.6578 \cdot 10^{-4}$	15.0	2.8	$3.5299 \cdot 10^{-4}$	7.8	2.6	$7.7484 \cdot 10^{-4}$	12.7	2.8	$5.6256 \cdot 10^{-4}$
130	23.0	2.7	$1.4593 \cdot 10^{-4}$	21.1	2.7	$1.8418 \cdot 10^{-4}$	14.5	2.6	$6.9964 \cdot 10^{-4}$	19.9	3.0	$8.7956 \cdot 10^{-5}$

increases with increasing SNCs-*g*-LA nanoparticles concentrations to 5 wt%. As can be seen from Table 1, the crystallization constant k increases with increasing SNCs-*g*-LA nanoparticles concentrations to 5 wt%. The addition of 5 wt% SNCs-*g*-LA nanoparticles in PLA induced more crystallization rate. Nevertheless, the value of *k* decreases with increasing grafted SNCs concentrations (7 wt%), indicating that the addition of more grafted SNCs causes hindrance in the diffusion of the PLA molecules, which results in a lower crystallization rate. Further, the effectiveness of SNCs-*g*-LA nanoparticles as a heterogeneous nucleating agent is studied by looking at the evolution of the $t_{1/2}$ as a function of T_c (Figure 7). The $t_{1/2}$ for both neat PLA and PLA nanocomposites starts to decrease with increasing T_c but increases further increases T_c. The minimum $t_{1/2}$ for neat PLA was found to be 10.4 min at T_c =110 °C. However, the addition of SNCs-*g*-LA nanoparticles decreases the minimum $t_{1/2}$ in all PLA nanocomposites irrespective of the concentration level. This implies that adding SNCs-*g*-LA nanoparticles not only significantly increases the kinetics of crystallization of PLA but also decreases the minimum T_c. Furthermore, the T_c of the all-PLA nanoparticles is lower than neat PLA. Interestingly, between different concentrations, 5 wt% of SNCs-*g*-LA nanoparticles content was found to have the lowest value of $t_{1/2}$ (3.9 min). Further, increasing the amount of SNCs-*g*-LA nanoparticles again increases the $t_{1/2}$ due to the decrease in the barrier-free energy.

3.5. The effect of SNCs-*g*-LA nanoparticles on the spherulite growth rate of PLA

To understand the effect of adding SNCs-*g*-LA nanoparticles on the spherulite growth rate (*SGR*) of PLA, *SGR* was monitored by using polarized optical microscopy (POM). Figure 8 shows the *SGR* as a function of T_c for neat PLA and PLA nanocomposites. According to the crystallization theory, the crystal growth rate shows a well-known Gaussian-shaped temperature dependence [43–45]. The Gaussian-shaped temperature dependence was observed for both neat PLA and PLA nanocomposites, as shown

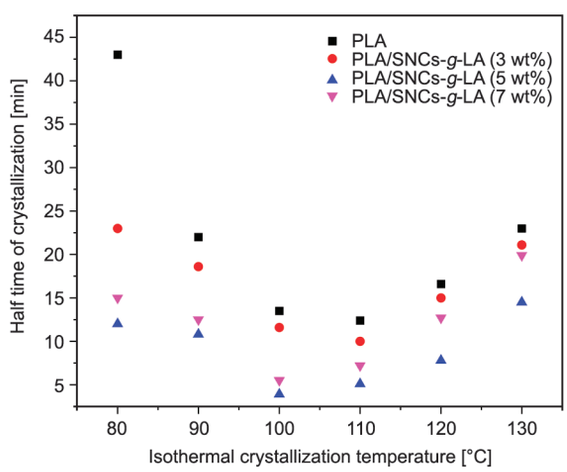

Figure 7. The $t_{1/2}$ of neat PLA and PLA nanocomposites with different concentrations of SNCs-*g*-LA nanoparticles.

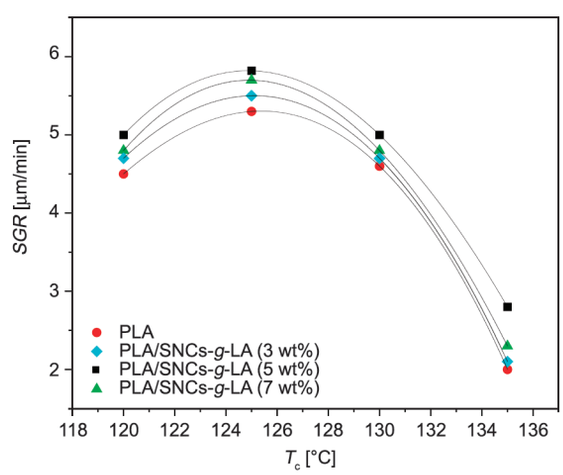

Figure 8. The spherulite growth rate of neat PLA and PLA nanocomposites was measured at different isothermal crystallization temperatures.

in Figure 8. Further, the *SGR* of PLA nanocomposites was higher than the neat PLA sample. Interestingly, the maximum *SGR* of PLA was found in the presence of 5 wt% of SNCs-*g*-LA nanoparticles compared to the PLA nanocomposites with the loading of 7 and 3 wt% SNCs-*g*-LA nanoparticles. This phenomenon can be explained by the competition between kinetic and thermodynamic crystallization for grafted SNCs as a nucleating agent at lower concentrations (5 wt%).

In addition, the spherulite morphology of neat and PLA nanocomposites was observed at T_c = 130 °C by using optical microscopy, and the results are shown in Figure 9. The results show regardless of the sample, the presence of the spherulites with maltase extinction crosses and can be seen in all pictures. However, whereas in the case of neat PLA the spherulite presence is limited compared (Figure 9a) to the SNCs-*g*-LA reinforced PLA composites. The PLA containing SNCs-*g*-LA nanoparticles show a smaller size and larger density of spherulite than neat PLA indicating the nucleation density has been significantly increased by grafted SNCs. It is worth noting that the morphology of spherulite is less compact and irregular in neat PLA. However, PLA/SNCs-*g*-LA nanocomposites indicate a compact and regular structure was observed.

3.6. Effect of SNCs-*g*-LA nanoparticles on the long period (L_{ac})

SAXS is an influential technique that probes the morphological changes of semicrystalline polymers such as PLA [19]. It can provide morphological information, such as long period (L_{ac}), the crystal layer thickness (L_c), and the amorphous layer thickness ($L_a = L_{ac} - L_c$). Therefore, SAXS technique is performed to observe the effect of the SNCs-*g*-LA nanoparticles on structural changes at various

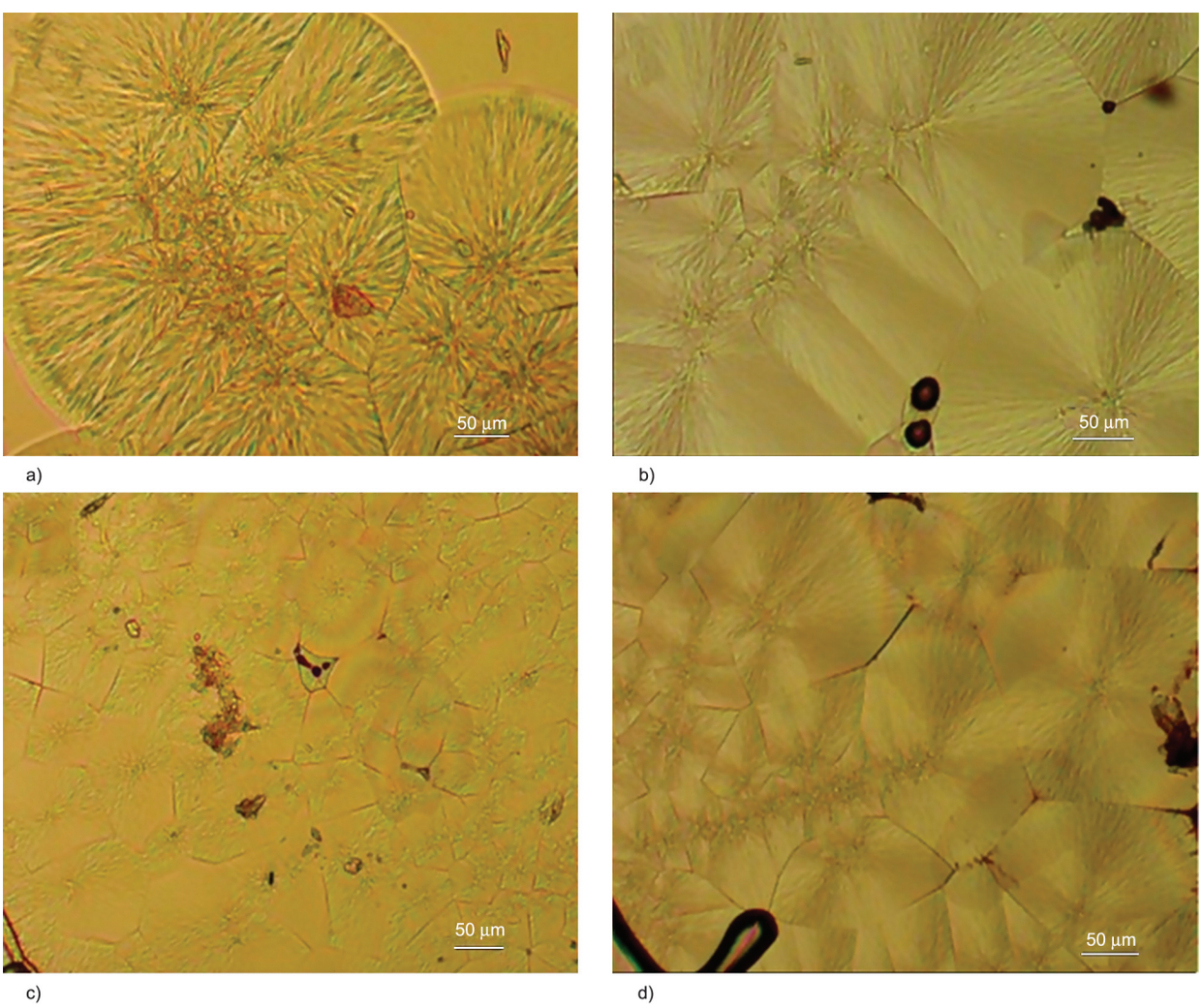

Figure 9. Spherulite morphology of a) neat PLA, b) PLA/SNCs-*g*-LA (3 wt%), c) PLA/SNCs-*g*-LA (5 wt%) and d) PLA/SNCs-*g*-LA (7 wt%) nanocomposites which measured at T_c = 130 °C.

crystallization temperatures. In order to obtain the morphological parameters, a single-dimensional correlation function is applied [12]. As can be seen in Figure 10, the SAXS patterns of both neat PLA and PLA nanocomposites are depended on the crystallization temperatures and increasing the annealing temperature yields noticeable changes in the SAXS correlation function plots. At 80 °C neither a peak nor shoulder is observed in the SAXS scattering pattern of PLA. However, when the T_c is increased from 80 to 100 °C, the SAXS peak begins to be visible, and SAXS intensity increases with a further increase of T_c. At T_c = 100 °C, a small shoulder appears at q = 0.31 nm^{-1}, corresponding to the long spacing of 18.5 nm. The maximum scattering vector (q_{max}) appears at 110 °C, which is shifted to a lower q_{max} value by increasing temperature up to 130 °C (0.28 nm^{-1}). This indicates that the T_c shifts the SAXS peaks to lower values and is increasing the long spacing period. Thus, a change in the thickness distribution of the lamellae and amorphous regions can be observed. The higher long period at 130 °C is probably due to the formation of secondary lamellae in the amorphous region, which decreases the size of the amorphous region. The PLA nanocomposite shows a similar SAXS profile. However, the position of scattering peak at all T_c is shifted to a smaller q_{max} compared to neat PLA. This decrement clearly affected the morphological parameters of PLA nanocomposites (Table 1). As can be seen in Table 1, the inclusion of 5 wt % grafted SNCs resulted in the increment of the L_{ac} as well as L_c. The L_{ac} and L_c values at the same crystallization temperature increase in PLA nanocomposites compared to neat PLA. In addition, the L_a values decrease at the same T_c for PLA nanocomposites. These results reveal that the grafted SNCs chains promote the PLA crystalline chain packing, which leads to an increase in crystal layer thickness and a decrease in the amorphous layer thickness. Also, a new peak begins to appear upon

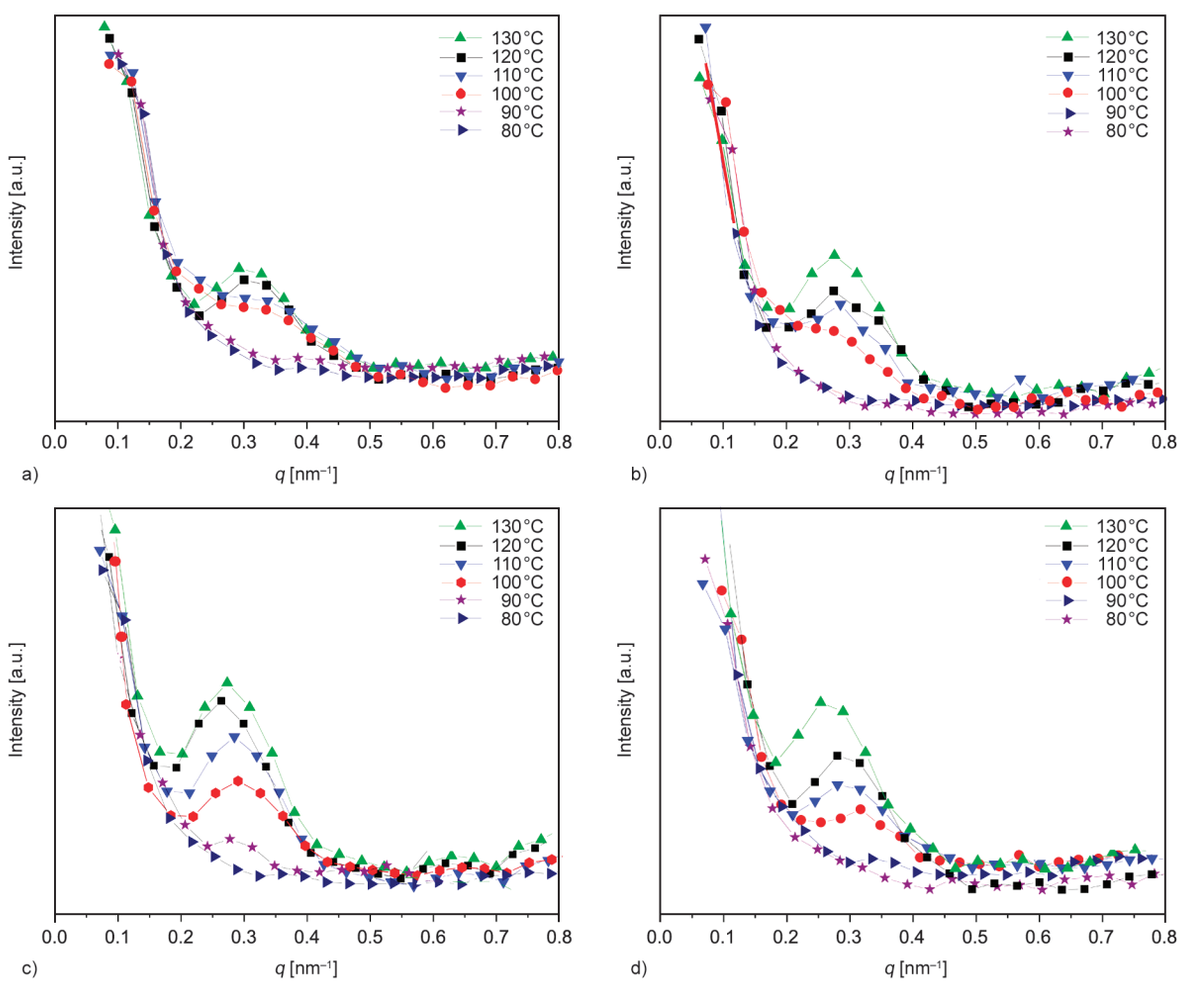

Figure 10. SAXS patterns of a) neat PLA, b) PLA/SNCs-*g*-LA (3 wt%), c) PLA/SNCs-*g*-LA (5 wt%), and d) PLA/SNCs-*g*-LA (7 wt%) nanocomposite which is crystallized at different isothermal crystallization temperatures.

annealing, which corresponds to the formation of secondary lamellae [26–28].

4. Conclusions

In this paper, the effect of SNCs-*g*-LA nanoparticles on the phase composition, phase transition, and crystallization behavior of PLA were explored. For this purpose, different concentrations of SNCs-*g*-LA (3, 5, and 7 wt%) were added to the PLA to obtain the PLA/SNCs-*g*-LA nanocomposite. It was found that the formation of α crystal in PLA nanocomposites is more likely than α′ crystal, and the rate of phase transition in all PLA nanocomposites was higher than in neat PLA. This phenomenon is more prominent in PLA nanocomposites with 5 wt% SNCs-*g*-LA nanoparticles. WAXS and DSC results confirm that by adding 5 wt% of SNCs-*g*-LA nanoparticles, the T_{trans} shifts to a lower temperature, and the degree of α crystal shifts to a higher value compared to other SNCs-*g*-LA nanoparticles concentrations. Moreover, POM observations revealed that PLA spherulites of α crystal were accelerated by the presence of SNCs-*g*-LA nanoparticles. The *SGR* where just α crystal was formed showed that the size of spherulite was smaller in PLA/SNCs-*g*-LA (5 wt%) nanocomposite compared to neat PLA. Furthermore, the half-time of crystallization ($t_{1/2}$) of PLA decreased with the addition of SNCs-*g*-LA nanoparticles. Interestingly, the $t_{1/2}$ of PLA was minimum by adding 5 wt% SNCs-*g*-LA nanoparticles, and it decreased from 10.4 to 3.9 min. Therefore, it can be concluded that 5 wt% SNCs-*g*-LA is an optimum concentration, and it can help both thermodynamically and kinetically to form more stable crystalline structure of PLA.

Acknowledgements

The authors would like to thank National Science and Engineering Research Council (NSERC) of Canada, Centre québecois des matériaux fonctionnels' or CQMF from Fonds de Recherche du Québec Nature et Technologie (FRQNT), and Center de recheche sur les systèmes polymèreset composites (CREPEC) for financial support.

References

[1] McKeown P., Jones M. D.: The chemical recycling of PLA: A review. Sustainable Chemistry, **1**, 1–22 (2020). https://doi.org/10.3390/suschem1010001

[2] Ghomi E. R., Khosravi F., Ardahaei A. S., Dai Y., Neisiany R. E., Foroughi F., Wu M., Das O., Ramakrishna S.: The life cycle assessment for polylactic acid (PLA) to make it a low-carbon material. Polymers, **13**, 1854 (2021). https://doi.org/10.3390/polym13111854

[3] Ilyas R. A., Sapuan S. M., Harussani M. M., Hakimi M. Y. A. Y., Haziq M. Z. M., Atikah M. S. N., Asyraf M. R. M., Ishak M. R., Razman M. R., Nurazzi N. M., Norrrahim M. N. F., Abral H., Asrofi M.: Polylactic acid (PLA) biocomposite: Processing, additive manufacturing and advanced applications. Polymers, **13**, 1326 (2021). https://doi.org/10.3390/polym13081326

[4] Tümer E. H., Erbil H. Y.: Extrusion-based 3D printing applications of PLA composites: A review. Coatings, **11**, 390 (2021). https://doi.org/10.3390/coatings11040390

[5] Gerometta M., Rocca-Smith J. R., Domenek S., Karbowiak T.: Physical and chemical stability of PLA in food packaging. in 'Reference Module in Food Science' Elsevier, Amsterdam, 1–11 (2019). https://doi.org/10.1016/B978-0-08-100596-5.22471-2

[6] Siracusa V., Rocculi P., Romani S., Rosa M. D.: Biodegradable polymers for food packaging: A review. Trends in Food Science and Technology, **19**, 634–643 (2008). https://doi.org/10.1016/j.tifs.2008.07.003

[7] Auras R. A., Singh S. P., Singh J. J.: Evaluation of oriented poly(lactide) polymers *vs*. existing PET and oriented PS for fresh food service containers. Packaging Technology and Science, **18**, 207–216 (2005). https://doi.org/10.1002/pts.692

[8] Auras R., Harte B., Selke S.: Effect of water on the oxygen barrier properties of poly(ethylene terephthalate) and polylactide films. Journal of Applied Polymer Science, **92**, 1790–1803 (2004). https://doi.org/10.1002/app.20148

[9] Zhang J., Tashiro K., Tsuji H., Domb A. J.: Disorder-to-order phase transition and multiple melting behavior of poly(L-lactide) investigated by simultaneous measurements of WAXD and DSC. Macromolecules, **41**, 1352–1357 (2008). https://doi.org/10.1021/ma0706071

[10] Zhang J., Tsuji H., Noda I., Ozaki Y.: Structural changes and crystallization dynamics of poly(L-lactide) during the cold-crystallization process investigated by infrared and two-dimensional infrared correlation spectroscopy. Macromolecules, **37**, 6433–6439 (2004). https://doi.org/10.1021/ma049288t

[11] Cocca M., di Lorenzo M. L., Malinconico M., Frezza V.: Influence of crystal polymorphism on mechanical and barrier properties of poly(L-lactic acid). European Polymer Journal, **47**, 1073–1080 (2011). https://doi.org/10.1016/j.eurpolymj.2011.02.009

[12] Sawai D., Yokoyama T., Kanamoto T., Sungil M., Hyon S-H., Myasnikova L. P.: Crystal transformation and development of tensile properties upon drawing of poly (L-lactic acid) by solid-state coextrusion: Effects of molecular weight. Macromolecular Symposia, **242**, 93–103 (2006).
https://doi.org/10.1002/masy.200651015

[13] Alemán C., Lotz B., Puiggali J.: Crystal structure of the α-form of poly(L-lactide). Macromolecules, **34**, 4795–4801 (2001).
https://doi.org/10.1021/ma001630o

[14] Bouapao L., Tsuji H.: Stereocomplex crystallization and spherulite growth of low molecular weight poly(L-lactide) and poly(D-lactide) from the melt. Macromolecular Chemistry and Physics, **210**, 993–1002 (2009)
https://doi.org/10.1002/macp.200900017

[15] Qiu Z., Li Z.: Effect of orotic acid on the crystallization kinetics and morphology of biodegradable poly(L-lactide) as an efficient nucleating agent. Industrial and Engineering Chemistry Research, **50**, 12299–12303 (2011).
https://doi.org/10.1021/ie2019596

[16] Jacobsen S., Fritz H. G.: Plasticizing polylactide-the effect of different plasticizers on the mechanical properties. Polymer Engineering and Science, **39**, 1303–1310 (1999).
https://doi.org/10.1002/pen.11517

[17] Xiao H., Yang L., Ren X., Jiang T., Yeh J-T.: Kinetics and crystal structure of poly(lactic acid) crystallized nonisothermally: Effect of plasticizer and nucleating agent. Polymer Composites, **31**, 2057–2068 (2010).
https://doi.org/10.1002/pc.21004

[18] Zhao B., Li L., Lu F., Zhai Q., Yang B., Schick C., Gao Y.: Phase transitions and nucleation mechanisms in metals studied by nanocalorimetry: A review. Thermochimica Acta, **603**, 2–23 (2015).
https://doi.org/10.1016/j.tca.2014.09.005

[19] Libster D., Aserin A., Garti N.: Advanced nucleating agents for polypropylene. Polymers for Advanced Technologies, **18**, 685–695 (2007).
https://doi.org/10.1002/pat.970

[20] Varga J., Mudra I., Ehrenstein G. W.: Highly active thermally stable β-nucleating agents for isotactic polypropylene. Journal of Applied Polymer Science, **74**, 2357–2368 (1999).
https://doi.org/10.1002/(SICI)1097-4628(19991205)74:10%3C2357::AID-APP3%3E3.0.CO;2-2

[21] Mathieu C., Thierry A., Wittmann J. C., Lotz B.: Specificity and versatility of nucleating agents toward isotactic polypropylene crystal phases. Journal of Polymer Science Part B: Polymer Physics, **40**, 2504–2515 (2002).
https://doi.org/10.1002/polb.10309

[22] Kristiansen M., Tervoort T., Smith P., Goossens H.: Mechanical properties of sorbitol-clarified isotactic polypropylene: Influence of additive concentration on polymer structure and yield behavior. Macromolecules, **38**, 10461–10465 (2005).
https://doi.org/10.1021/ma0517401

[23] Mohmeyer N., Schmidt H-W., Kristiansen P. M., Altstädt V.: Influence of chemical structure and solubility of bisamide additives on the nucleation of isotactic polypropylene and the improvement of its charge storage properties. Macromolecules, **39**, 5760–5767 (2006).
https://doi.org/10.1021/ma060340q

[24] Luo F., Wang K., Ning N., Geng C., Deng H., Chen F., Fu Q., Qian Y., Zheng D.: Dependence of mechanical properties on β-form content and crystalline morphology for β-nucleated isotactic polypropylene. Polymers for Advanced Technologies, **22**, 2044–2054 (2011).
https://doi.org/10.1002/pat.1718

[25] Abe H., Kikkawa Y., Inoue Y., Doi Y.: Morphological and kinetic analyses of regime transition for poly[(S)-lactide] crystal growth. Biomacromolecules, **2**, 1007–1014 (2001).
https://doi.org/10.1021/bm015543v

[26] Xu J-Z., Chen T., Yang C-L., Li Z-M., Mao Y-M., Zeng B-Q., Hsiao B. S.: Isothermal crystallization of poly(L-lactide) induced by graphene nanosheets and carbon nanotubes: A comparative study. Macromolecules, **43**, 5000–5008 (2010).
https://doi.org/10.1021/ma100304n

[27] Lai W-C.: Thermal behavior and crystal structure of poly(L-lactic acid) with 1,3:2,4-dibenzylidene-D-sorbitol. The Journal of Physical Chemistry: B, **115**, 11029–11037 (2011).
https://doi.org/10.1021/jp2037312

[28] Pan P., Liang Z., Nakamura N., Miyagawa T., Inoue Y.: Uracil as nucleating agent for bacterial poly[(3-hydroxybutyrate)-*co*-(3-hydroxyhexanoate)] copolymers. Macromolecular Bioscience, **9**, 585–595 (2009).
https://doi.org/10.1002/mabi.200800294

[29] Muller J., González-Martínez C., Chiralt A.: Combination of poly(lactic) acid and starch for biodegradable food packaging. Materials, **10**, 952 (2017).
https://doi.org/10.3390/ma10080952

[30] Mandala R., Bannoth A. P., Akella S., Rangari V. K., Kodali D.: A short review on fused deposition modeling 3D printing of bio□based polymer nanocomposites. Journal of Applied Polymer Science, **14**, 51904 (2022).
https://doi.org/10.1002/app.51904

[31] Zamir S. S., Fathi B., Ajji A., Robert M., Elkoun S.: Crystallinity and gas permeability of poly (lactic acid)/starch nanocrystal nanocomposite. Polymers, **14**, 2802 (2022).
https://doi.org/10.3390/polym14142802

[32] Ke T., Sun X.: Melting behavior and crystallization kinetics of starch and poly(lactic acid) composites. Journal of Applied Polymer Science, **89**, 1203–1210 (2003).
https://doi.org/10.1002/app.12162

[33] Campelo P. H., Sant'Ana A. S., Clerici M. T. P. S.: Starch nanoparticles: Production methods, structure, and properties for food applications. Current Opinion in Food Science, **33**, 136–140 (2020).
https://doi.org/10.1016/j.cofs.2020.04.007

[34] Zamir S. S., Frouzanmehr M. R., Nagalakshmaiah M., Ajji A., Robert M., Elkoun S.: Chemical compatibility of lactic acid-grafted starch nanocrystals (SNCs) with polylactic acid (PLA). Polymer Bulletin, **76**, 3481–3499 (2019). https://doi.org/10.1007/s00289-018-2548-y

[35] Jang W. Y., Shin B. Y., Lee T. J., Narayan R.: Thermal properties and morphology of biodegradable PLA/starch compatibilized blends. Journal of Industrial and Engineering Chemistry, **13**, 457–464 (2007).

[36] Zhang J-F., Sun X.: Mechanical properties of poly(lactic acid)/starch composites compatibilized by maleic anhydride. Biomacromolecules, **5**, 1446–1451 (2004). https://doi.org/10.1021/bm0400022

[37] Yu J., Ai F., Dufresne A., Gao S., Huang J., Chang P. R.: Structure and mechanical properties of poly(lactic acid) filled with (starch nanocrystal)-graft-poly(ε-caprolactone). Macromolecular Materials and Engineering, **293**, 763–770 (2008). https://doi.org/10.1002/mame.200800134

[38] Zhang J., Duan Y., Sato H., Tsuji H., Noda I., Yan S., Ozaki Y.: Crystal modifications and thermal behavior of poly(L-lactic acid) revealed by infrared spectroscopy. Macromolecules, **38**, 8012–8021 (2005). https://doi.org/10.1021/ma051232r

[39] Pan P., Zhu B., Kai W., Dong T., Inoue Y.: Effect of crystallization temperature on crystal modifications and crystallization kinetics of poly(L-lactide). Journal of Applied Polymer Science, **107**, 54–62 (2007). https://doi.org/10.1002/app.27102

[40] Marseglia E. A.: Kinetic theory of crystallization of amorphous materials. Journal of Non-Crystalline Solids, **41**, 31–36 (1980). https://doi.org/10.1016/0022-3093(80)90188-X

[41] Hoffman J. D., Weeks J. J.: Melting process and the equilibrium melting temperature of polychlorotrifluoroethylene. Journal of Research of the National Bureau of Standards Section A: Physics and Chemistry, **66**, 13–28 (1962). https://doi.org/10.6028/jres.066A.003

[42] Avrami M.: Kinetics of phase change. I General theory. The Journal of Chemical Physics, **7**, 1103–1112 (1939). https://doi.org/10.1063/1.1750380

[43] Xu H-S., Dai X. J., Lamb P. R., Li Z-M.: Poly(L-lactide) crystallization induced by multiwall carbon nanotubes at very low loading. Journal of Polymer Science Part B: Polymer Physics, **47**, 2341–2352 (2009). https://doi.org/10.1002/polb.21830

[44] Saeidlou S., Huneault M. A., Li H., Park C. B.: Poly (lactic acid) crystallization. Progress in Polymer Science, **37**, 1657–1677 (2012). https://doi.org/10.1016/j.progpolymsci.2012.07.005

[45] di Lorenzo M. L., Androsch R.: Influence of α′-/α-crystal polymorphism on properties of poly(L-lactic acid). Polymer International, **68**, 320–334 (2019). https://doi.org/10.1002/pi.5707

[46] Zamir S. S., Fathi B., Ajji A., Robert M., Elkoun S.: Biodegradation of modified starch/poly lactic acid nanocomposite in soil. Polymer Degradation and Stability, **109**, 109902 (2022). https://doi.org/10.1016/j.polymdegradstab.2022.109902

[47] Namazi H., Dadkhah A.: Convenient method for preparation of hydrophobically modified starch nanocrystals with using fatty acids. Carbohydrate Polymers, **79**, 731–737 (2010). https://doi.org/10.1016/j.carbpol.2009.09.033